ELSEVIER

Nuclear Physics B 495 [FS] (1997) 583–607

NUCLEAR PHYSICS B

Geometrical folding transitions of the triangular lattice in the face-centred cubic lattice

M. Bowick [a,1], O. Golinelli [b,2], E. Guitter [b,3], S. Mori [c,4]

[a] *Physics Department, Syracuse University, Syracuse, NY 13244-1130, USA*

[b] *CEA, Service de Physique Théorique de Saclay, F-91191 Gif sur Yvette Cedex, France*

[c] *Department of Physics, Graduate School of Science, University of Tokyo, Hongo 7-3-1, Bunkyo-ku, Tokyo 113, Japan*

Received 20 November 1996; accepted 13 March 1997

Abstract

We study the folding of the regular two-dimensional triangular lattice embedded in the regular three-dimensional Face-Centred Cubic lattice, a discrete model for the crumpling of phantom membranes. Possible folds are complete planar folds, folds with the angle of a regular tetrahedron (71°) or with that of a regular octahedron (109°). We study this model in the presence of a *negative* bending rigidity K, which favours the folding process. We use both a cluster variation method (CVM) approximation and a transfer matrix approach. The system is shown to undergo two separate geometrical transitions with increasing $|K|$: a first discontinuous transition separates a phase where the triangular lattice is preferentially wrapped around octahedra from a phase where it is preferentially wrapped around tetrahedra. A second continuous transition separates this latter phase from a phase of complete folding of the lattice on top of a single triangle. © 1997 Elsevier Science B.V.

PACS: 05.90.+m; 87.22.Bt

Keywords: Folding; Crumpling; Phase transition; Bending rigidity; Membrane

[1] E-mail: bowick@npac.syr.edu

[2] E-mail: golinelli@spht.saclay.cea.fr

[3] E-mail: guitter@spht.saclay.cea.fr

[4] E-mail: mori@monet.phys.s.u-tokyo.ac.jp

PII S0550-3213(97)00198-3

1. Introduction

The statistical mechanics of membranes and flexible two-dimensional interfaces is an extremely rich and rather challenging field [1,2]. Of fundamental importance is the phase diagram of such systems and the precise nature of the remarkable orientationally ordered phases that they possess. Faced with a difficult problem it is often useful to explore extreme limits. One such limit is that of a flexible phantom fixed-connectivity membrane with infinite elastic stiffness. In this limit the in-plane "phonon" degrees of freedom are frozen, leaving only out-of-plane "bending" modes. In a $1/d$ expansion (where d is the dimension of the embedding space) such a membrane exhibits a continuous crumpling transition at a positive critical bending rigidity [3].

Discretising this type of membrane as a triangular lattice leads to a model of the statistical mechanics of folding. Finally one can discretise the space of allowed local folds to obtain a completely discrete "vertex" model. The simplest case is planar folding, in which the local folds are no-folds or complete folds [4–6]. This corresponds to folding the triangular lattice onto itself. Planar folding admits many equivalent representations, each of them interesting. It may be formulated as an 11-vertex model equivalent to the three-colouring problem of a triangular lattice [5,6]. For zero bending rigidity this model was solved by Baxter, in its dual formulation, as the combinatorics of edge-colourings of the honeycomb lattice [7]. It may also be mapped to the fully packed loop model with fugacity 2 describing non-intersecting loops on a honeycomb lattice such that every vertex is covered by a loop [8,9]. Finally an interpretation of the Z_3 colour variable as a Potts spin living on the centres of the bonds maps planar folding to a description of the ground state of the three-state antiferromagnetic Potts model on the Kagomé lattice [10]. Adding a positive bending rigidity to the planar folding model one finds a first-order phase transition to a completely unfolded phase [6,11].

Since planar folding is very restrictive, it is natural to consider enlarging the discrete space of allowed folds. In Ref. [12] planar folding was generalised to a particular three-dimensional folding allowing four types of discrete folds. This corresponds to choosing the embedding space to be a three-dimensional Face-Centred Cubic lattice. This 3D folding model has a formulation as a 96-vertex statistical mechanics model and, once again, undergoes a first-order transition to an ordered phase at a definite positive bending rigidity [13,14]. It also admits a formulation as a dressed three-colouring problem [12].

In this paper we extend the study of the 96-vertex model to *negative* bending rigidity. In such a model folding is energetically favoured. Negative bending rigidity might in principle be realisable in a polymerised membrane with strong attractive next-to-nearest neighbour interactions [15] or for a membrane in a sufficiently bad solvent. Of course the model we treat is unphysical in that we neglect self-avoidance. Nevertheless we believe that the richness of the phantom problem itself is more than sufficient justification for a detailed study. The inclusion of self-avoidance is challenging, as in all attempts to model physical membranes, and remains in the present case an open problem.

Utilising both the cluster variation method and a transfer matrix formalism we find two distinct geometrical phase transitions at negative bending rigidity. As K becomes more

negative starting from zero, there is a first-order transition from a phase of preferential octahedral wrapping to a phase with preferential tetrahedral wrapping, followed by a continuous piling transition to a single plaquette. We determine a set of three order parameters that completely characterise the separate phases observed.

The outline of the paper is as follows. In Section 2 we review the construction of the 96-vertex model. In Section 3 we discuss four natural submodels of the 96-vertex model – these correspond to different restrictions on the allowed folds. We also introduce a duality transformation which maps any allowed folding configuration to another allowed folding configuration. In Section 4 we study the statistics of folding for negative bending rigidity and introduce the three geometrical order parameters. The phase diagram is determined by the Cluster Variation Method (CVM) and by a transfer matrix method. In Section 5 we discuss the incorporation of external fields. Finally we summarise our results and their significance in Section 6.

2. The 96-vertex model

2.1. General definition of the folding model

In this section, we first recall the model of discrete folding of the regular 2-dimensional triangular lattice embedded in the regular 3-dimensional Face-Centred Cubic (FCC) lattice. A detailed derivation of the model can be found in Ref. [12]. As explained below, the model is easily expressible in terms of *two* Z_2 *variables* σ and z, defined on the faces of the triangular lattice. The associated domain walls indicate the different types of folds. The spin variables σ and z are subject to *two basic folding rules*, leading to a re-expression of the model as a *96-vertex* model on the triangular lattice.

A folding of the triangular lattice in the FCC lattice is simply a mapping which assigns to each vertex of the triangular lattice a vertex in the FCC lattice, with the constraint that neighbouring vertices on the triangular lattice are sent to nearest neighbours in the FCC lattice. The FCC lattice can be viewed as consisting of a filling of space by regular octahedra complemented by regular tetrahedra (see Fig. 1). Nearest-neighbour triplets in the FCC lattice thus form equilateral triangles. In the folding process each elementary triangle of the triangular lattice is mapped onto one of these equilateral triangles of the FCC lattice. Fig. 2 shows an example of folding of a piece of triangular lattice consisting of an elementary hexagon excised from the lattice.

After folding, two adjacent triangles form some relative angle, i.e. their common link serves as a hinge and may be (partially) folded or not. There are four possible relative positions for two given neighbouring triangles, as depicted in Fig. 3, measured simply by the angle θ of the corresponding fold:

(i) $\theta = 180°$ – no fold: the triangles are side by side;
(ii) $\theta = 0°$ – complete fold: the triangles are on top of each other;
(iii) $\theta = \arccos(\frac{1}{3}) \sim 71°$ – fold with acute angle: the two triangles lie on the same tetrahedron, and

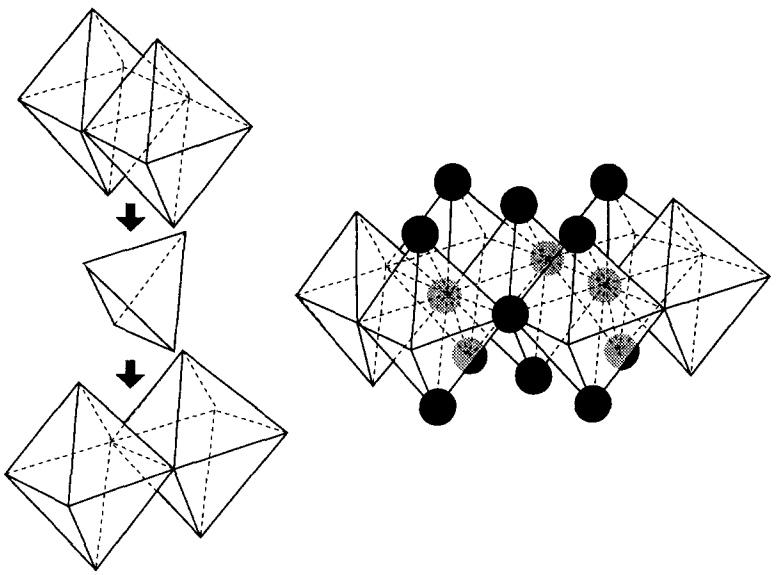

Fig. 1. The Face-Centred Cubic lattice viewed as a packing of 3D space with octahedra and tetrahedra.

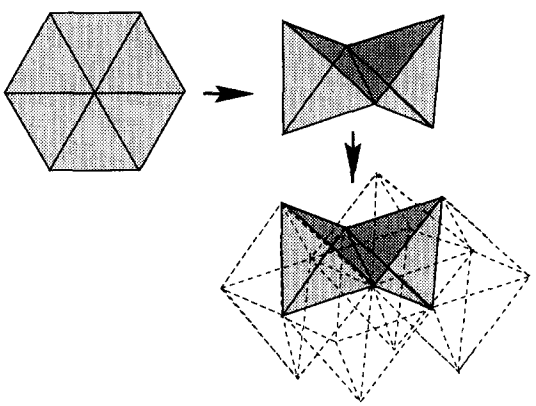

Fig. 2. An example of folding in the FCC lattice of an elementary hexagon cut out from the triangular lattice. Nearest neighbours in the hexagon remain nearest neighbours after embedding in the FCC lattice.

(iv) $\theta = \arccos(-\frac{1}{3}) \sim 109°$ – fold with obtuse angle: the triangles lie on the same octahedron.

It has been shown in Ref. [12] that these four possible types of folds are actually organised as the domain walls for two Z_2 variables $\sigma = \pm 1$ and $z = \pm 1$ defined on each face of the triangular lattice. The relative value of both z_2/z_1 and σ_2/σ_1 for two neighbouring triangles indicate which type of fold they form, with the correspondence displayed in Table 1. The domain walls for the z variable are the location of the folds which are either acute or obtuse, whereas those for the σ variable are the location of the folds which are either complete or obtuse. The superposition of these two types of domain wall fixes the folding state of all the links, specifying the folding state of the

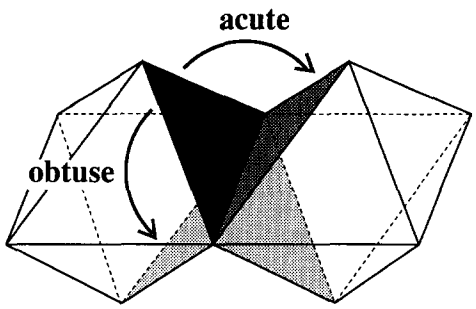

Fig. 3. The four possible folding angles between two adjacent triangles. The neighbour of the dark triangle may (i) occupy the symmetric position in the same plane (no fold), (ii) be itself on top of the dark triangle (complete fold), (iii) lie on the same tetrahedron (i.e. form an acute angle), (iv) lie on the same octahedron (i.e. form an obtuse angle).

Table 1
The relative folding state of two neighbouring triangles according to their relative values of $z_i = \pm 1$ and $\sigma_i = \pm 1$ $(i = 1, 2)$

z_2/z_1	σ_2/σ_1	Angle
1	1	no fold
1	−1	complete fold
−1	1	acute fold
−1	−1	obtuse fold

lattice (up to a global orientation).

Note, of course, that the two global symmetries $\sigma \to -\sigma$ and $z \to -z$, independently, leave the folding invariant.

2.2. *The two basic folding rules*

With the above definitions, the σ and z variables on neighbouring triangles are not totally independent. This can be seen by considering the folding of any elementary hexagon made of six neighbouring triangles in the lattice. The relative positions of the six surrounding vertices of the hexagon can be traced back from the folds of its six internal links. After a complete turn around the hexagon, the same absolute position must be found for any of these six vertices. This leads to two basic folding rules for the values σ_i and z_i $(i = 1, \ldots, 6)$ on these six triangles (see Fig. 4).

The first rule involves the variable σ only and states that

$$\sum_{i=1}^{6} \sigma_i = 0 \bmod 3. \tag{2.1}$$

This rule is easily understood in terms of 3-colourability of the links of the triangular lattice as follows. When embedded in the FCC lattice, the links of the triangular lattice must belong to one of the three crystalline planes (200), (020) or (002) which cross

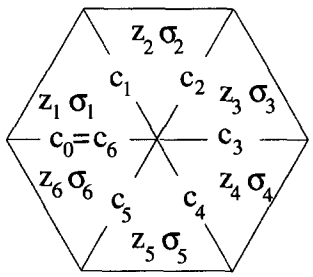

Fig. 4. The six z_i and σ_i variables around a given vertex, and the colours c_i of the interior links.

the octahedra by their three square bases. If we assign a colour to each of these three planar directions and colour the links of the FCC lattice correspondingly, this induces a 3-colouring of the triangular lattice links with three colours ($c = 0, 1, 2 \bmod 3$), which, moreover, have to be distinct on the three edges of the elementary triangles. One can easily check that the colours c_i of the six interior links of a hexagon (see Fig. 4) are directly linked to the σ_i variables by

$$c_j - c_i = \sum_{k=i+1}^{j} \sigma_k \bmod 3. \tag{2.2}$$

For instance, if $\sigma_2/\sigma_1 = -1$, then $c_2 - c_0 = \sigma_1 + \sigma_2 = 0$ since a complete or an obtuse fold puts the link 2 in the same crystalline plane as the link 0. The first basic folding rule simply states that the same colour must be found after a complete turn around the hexagon, i.e. that $c_0 = c_6$.

This first rule on the σ variable is not sufficient to ensure that the (z_i, σ_i) do correspond to an actual folded state of the hexagon. This is because the colour only partially specifies the actual orientation of the links in 3-dimensional space. A second basic folding rule involves both the z and σ variables and can be stated as follows:

$$\prod_{i \in I(c)} z_i z_{i+1} = 1, \qquad \text{for } c = 0, 1, 2,$$

$$I(c) = \left\{ i : \sum_{k=1}^{i} \sigma_k = c \bmod 3 \right\}. \tag{2.3}$$

This rule states that the number of changes of the z variable (which indicate folds which are either obtuse or acute) occurring on all interior links of a given colour in the hexagon must be even. The interpretation of this second rule will be clarified in Section 3 by use of a duality transformation. A direct interpretation based on the tetrahedral group can be found in Ref. [12].

It can be shown that the two rules (2.1) and (2.3), applied independently to all the hexagons of the original triangular lattice, are necessary and sufficient to define a folded state in the FCC lattice. Of course, our definition of folding does not impose any restrictions on possible self-intersections of the triangular lattice, which is therefore

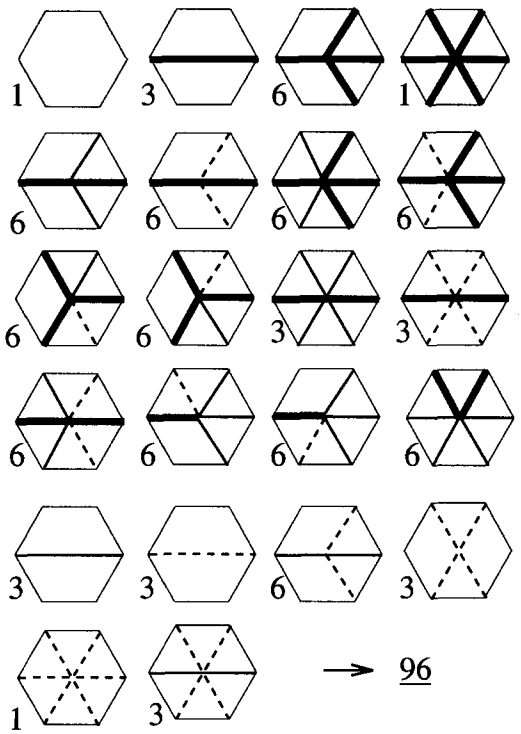

Fig. 5. The 96 possible hexagonal configurations around a vertex of the triangular lattice. Complete folds are represented by thick solid lines, obtuse folds by thin solid lines, and acute folds by dashed lines. We have represented only the vertices which are not equivalent to each other by a simple rotation. We indicate for each vertex the corresponding degeneracy under rotation.

considered as a phantom object. In the above formulation, the folding problem can thus be understood as a *constrained* system of two Z_2 variables z and σ.

It is interesting to work out all possible hexagonal configurations around a vertex allowed by the two rules (2.1) and (2.3). If one forgets the global fourfold symmetry under global reversal of all σ or z and represents only the corresponding domain walls, i.e. the four types of folds (i)–(iv) discussed above, one is led to 96 possible hexagonal configurations for any of the vertices of the triangular lattice. These are represented in Fig. 5. Our folding problem can thus be thought of as a *96-vertex model* defined on the triangular lattice.

2.3. *The folding energy*

For each type of fold, we introduce the folding energy

$$E = K\cos(\theta), \tag{2.4}$$

where θ is the angle of the fold (180° for no fold, 0° for a complete fold, 71° for an acute fold and 109° for an obtuse fold). The parameter K is the bending rigidity. In the following we shall be interested mainly in the case of *negative* K, which corresponds to

favouring folds. In terms of the variables σ_1, σ_2 and z_1, z_2 of the two triangles forming the fold, the energy simply reads

$$E = -\tfrac{1}{3}K\sigma_1\sigma_2(1 + 2z_1z_2). \tag{2.5}$$

The total folding energy is the sum of all elementary folding energies for all links of the triangular lattice.

3. Submodels and duality

In this section, we first introduce four submodels of the 96-vertex model describing four particular restricted folding problems. These models can be seen as particular limiting cases of the full 3D folding problem, where some particular *complete* ordering is realised in the folding process, which correspond to a restriction of the target space to subsets of the FCC lattice. We shall see in the next section that similar *partial* orderings occur spontaneously in the unrestricted full 3D folding problem. We also derive here a duality relation for the 96-vertex model.

3.1. Planar folding: an 11-vertex model

A first submodel can be obtained by restricting the target space to a single plane made of triangles in the FCC, say the crystalline plane (111) which cuts the FCC lattice along a regular 2-dimensional triangular lattice. In this case, we are dealing with the pure 2-dimensional folding problem studied in Refs. [4–6]. Here, only complete folds or no-folds are allowed. The model can thus be characterised by

$$z = +1 \tag{3.1}$$

globally on all triangles of the lattice (of course the choice + is arbitrary and a solution with $z = -1$ globally would be equally acceptable). With this constraint, the second folding rule (2.3) is automatically satisfied and the problem translates into a model with a single variable σ constrained by the folding rule (2.1). This model has been studied extensively in Ref. [5]. In particular, the number of folded states of a lattice of N triangles is found to grow like q^N with $q = \sqrt{3}\,\Gamma(\frac{1}{3})^{3/2}/2\pi \sim 1.208$. In terms of vertices, the model leads to 11 allowed vertices, which are those of the first row in Fig. 5.

3.2. Folding on a single octahedron: a 16-vertex model

One can restrict the target space to a single octahedron in the FCC lattice by simply allowing complete and obtuse folds only. Such folds are characterised by a change in the value of σ on neighbouring triangles. It is thus convenient to introduce a *staggered* variable by dividing the original triangular lattice in the two subsets A and B made

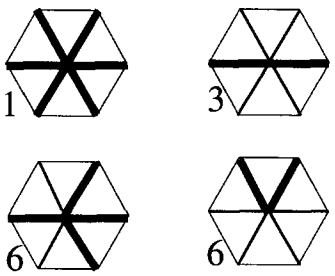

Fig. 6. The 16 vertices made of complete and obtuse folds only, characterising the folding on a single octahedron.

of all triangles pointing up and all triangles pointing down respectively in the original (unfolded) triangular lattice. We define

$$\sigma_{\rm st} = \begin{cases} \sigma, & \text{on subset A,} \\ -\sigma, & \text{on subset B.} \end{cases} \tag{3.2}$$

The submodel can then be simply characterised by

$$\sigma_{\rm st} = +1 \tag{3.3}$$

globally on the triangular lattice. With this constraint, the first folding rule is automatically satisfied since $\sum_{i=1}^{6} \sigma_i = 0$ on all hexagons. The second folding rule takes a particularly simple form since Eq. (3.3) imposes that the interior links of any particular hexagon take only two colours, say 0 and 1, which alternate such that $I(0) = \{1,3,5\}$ and $I(1) = \{2,4,6\}$. The rule (2.3) then translates into a single equation:

$$\prod_{i=1}^{6} z_i = 1. \tag{3.4}$$

The two rules (3.3) and (3.4) leave us with the 16 vertices of Fig. 6, where the thin lines (obtuse folds) indicate the domain walls of the z variable. One can easily show that the number of allowed folding configurations for N triangles grows like q^N, with $q = \sqrt{2}$. Indeed, all the entropy comes from the z degree of freedom and the constraint (3.4) is solved by introducing Z_2 variables $\eta = \pm 1$ on the *vertices* of the triangular lattice and requiring that the variable z on a given triangle is the product of the three η variables on the three surrounding vertices. In this formulation the variables η are not constrained, leading to $2^{N/2}$ configurations for the $\frac{1}{2}N$ vertices of the lattice.

3.3. Folding on a single tetrahedron: an 11-vertex model

A third submodel corresponds to the folding on a single tetrahedron, meaning only complete and acute folds are allowed. The model can be characterised simply by requiring that

$$z = +\sigma_{\rm st} \tag{3.5}$$

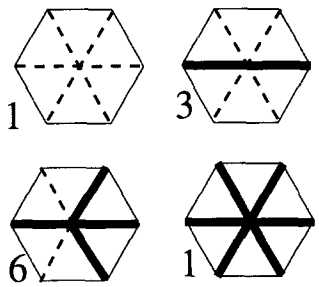

Fig. 7. The 11 vertices made of complete and acute folds only, characterising the folding on a single tetrahedron.

for all triangles in the lattice, with σ variables satisfying the first folding rule (2.1). Note that here again, (3.5) automatically implies the second folding rule (2.3) so that no extra constraint has to be imposed on the σ variables. In other words, for σ variables satisfying the first folding rule (2.1), the condition

$$\prod_{i\in I(c)} (\sigma_{\rm st})_i (\sigma_{\rm st})_{i+1} = \prod_{i\in I(c)} (-\sigma_i \sigma_{i+1}) = 1 \tag{3.6}$$

is automatically satisfied. This property can be checked directly by inspection of the 22 sets of σ_i satisfying the first folding rule. In our context, it can be understood simply as follows: given an arbitrary hexagonal configuration of σ variables around a vertex, satisfying the first basic folding rule, this configuration defines a particular *planar* folded state in, say, the (111) plane[5]. Given an arbitrary colour c, the image in the FCC lattice of the central vertex of the hexagon belongs to exactly one plane of the chosen colour. The (111) plane intersects this plane through a line of the chosen colour. Successive triangles around the hexagon can lie on the same side of this line or not. The passage from one side to the other takes place on a link of the chosen colour c and requires no fold, characterised by no change in σ, i.e. by a change in $\sigma_{\rm st}$. The number of changes in $\sigma_{\rm st}$ occurring on links of the colour c thus indicates the total number of crossings of the line when making a turn around the hexagon. This number must clearly be even since one must get back to the same side after one turn. This leads to (3.6).

The submodel of folding on a single tetrahedron is restricted to the 11 vertices displayed in Fig. 7, made of acute and complete folds only. These vertices are in direct correspondence with those of the planar 11-vertex model by replacing no-folds by acute folds. This is a particular example of the duality transformation discussed below.

3.4. Folding on a single triangle: a 1-vertex model

Finally, the three submodels above share a common vertex with all folds being complete, characterised by $z = \sigma_{\rm st} = +1$ everywhere. This trivial case describes a

[5] This planar folded state and the tetrahedral folded state will be dual to each other under the duality transformation described in the next section.

Table 2
Different submodels of the 96-vertex model

σ variable	z variable	Target space	Vertices	Dual model
$\sum_{i=1}^{6} \sigma_i = 0 \bmod 3$	$z = +1$	single plane	11	single tetrahedron
$\sigma_{st} = +1$	$\prod_{i=1}^{6} z_i = 1$	single octahedron	16	self-dual
$\sum_{i=1}^{6} \sigma_i = 0 \bmod 3$	$z = +\sigma_{st}$	single tetrahedron	11	single plane
$\sigma_{st} = +1$	$z = +1$	single triangle	1	self-dual

state of complete folding of the triangular lattice on top of a single triangle.

The above results are summarised in Table 2, which lists for each submodel the corresponding rules for the σ and z variables, the restricted target space and the associated number of vertices.

3.5. *The duality transformation*

Given any folded state characterised by its σ and z variables satisfying the two basic folding rules around all hexagons, we have seen that the first rule automatically implies Eq. (3.6). Multiplying this equation with the second folding rule on the z variables, we get

$$\prod_{i \in I(c)} (z\sigma_{st})_i (z\sigma_{st})_{i+1} = 1, \tag{3.7}$$

indicating that the global transformation

$$(\sigma, z) \rightarrow (\sigma, w \equiv z\sigma_{st}) \tag{3.8}$$

maps any folded state of the triangular lattice to another equally acceptable folded state. We shall refer to the above transformation as the duality transformation of the 96-vertex model. It is clearly an involution, since $\sigma_{st}^2 = 1$, and corresponds geometrically to a global interchange of all acute folds and no-folds.

It is interesting to look at the behavior of the different submodels of the previous subsection under the duality transformation. The 16-vertex model is self-dual in the strong sense that any of its vertices is invariant under the duality transformation. The 11-vertex model describing the planar folding problem and that describing tetrahedral folding are dual to each other. In particular the study of Ref. [5] on the 2D folding problem applies to the tetrahedral folding problem as well. The duality transformations of the different submodels are shown in Table 2.

Finally, let us discuss again the meaning of the second folding rule (2.3). By duality, this second rule is totally equivalent to (3.7). Now (3.7) simply expresses that the number of changes in the variable $z\sigma_{st}$ occurring on the links of a given colour must be even. Such changes account for obtuse folds or no-folds, which are precisely the two ways of *crossing* the crystalline plane of the given colour. The number of such crossings on a loop must clearly be even, implying Eq. (3.7).

To conclude this section, we would like to mention that the duality transformation is a particular case of a more general group transformation for the allowed z configurations *at a fixed σ global configuration* satisfying the first folding rule (2.1). Indeed, given two folded states (σ, z) and (σ, z') defined on the entire lattice with the same σ, the configuration (σ, zz') also defines an allowed folded state, as is clear from the multiplicative nature of the second folding rule (2.3). The duality transformation simply corresponds to the allowed configuration $z' = \sigma_{\rm st}$.

4. Geometrical folding transitions

In this section, we will study the statistics of folding in the case of *negative* bending rigidity K. We will be interested primarily in the three following average values:

$$O \equiv \langle \sigma_{\rm st} \rangle, \qquad T \equiv \langle z\sigma_{\rm st} \rangle, \qquad P \equiv \langle z \rangle, \tag{4.1}$$

with of course $-1 \leqslant P, O, T \leqslant 1$. The average is taken over both all folded configurations and all triangles in the lattice. Following Table 2, we will refer to P, O and T as the planar, octahedral and tetrahedral order parameter respectively, since $P = 1$ (respectively $O = 1$ and $T = 1$) indicates a situation of pure planar folding (respectively folding on a single octahedron and folding on a single tetrahedron). A non-zero value of P will thus be the signature that the triangular lattice preferentially stays within planes of the FCC lattice. Similarly, we will interpret a non-zero value of O (respectively T) as a tendency for the triangular lattice to be preferentially wrapped around octahedra (respectively tetrahedra).

We will also consider two-point functions such as

$$O2 \equiv \langle (\sigma_{\rm st})_1 \, (\sigma_{\rm st})_2 \rangle, \qquad T2 \equiv \langle (z\sigma_{\rm st})_1 \, (z\sigma_{\rm st})_2 \rangle, \qquad P2 \equiv \langle z_1 z_2 \rangle, \tag{4.2}$$

for the correlations on two neighbouring triangles in the lattice.

4.1. The CVM approximation

The Cluster Variation Method (CVM) is an approximation of the exact variational formulation of the problem [16–18]. Consider our system of variables z, σ on the lattice and the energy (2.5) summed over all pairs of neighbouring triangles. In terms of a density matrix $\rho(\{\sigma, z\})$ for each *allowed* global folding configuration $\{\sigma, z\}$, the exact free energy F of the system can be obtained from

$$F = \Big[\sum_{\{\sigma,z\}} \rho(\{\sigma, z\}) [E(\{\sigma, z\}) + \ln \rho(\{\sigma, z\})] \Big]_{\rm min}. \tag{4.3}$$

Here we absorb the temperature factors $k_{\rm B}T$ in the definition of E and F. The subscript min means that the expression is taken at its minimum with respect to $\rho(\{\sigma, z\})$, with the normalisation constraint

$$\sum_{\{\sigma,z\}} \rho(\{\sigma,z\}) = 1. \tag{4.4}$$

This is the well-known variational principle. Average values are calculated according to

$$\langle A(\{\sigma,z\})\rangle = \sum_{\{\sigma,z\}} \rho_{\min}(\{\sigma,z\})\, A(\{\sigma,z\}), \tag{4.5}$$

where $\rho_{\min}(\{\sigma,z\})$ is the density at the minimum of the free energy functional (4.3).

The CVM approximation is obtained by truncating the generalised cumulant expansion for the entropy part of (4.3), $S \equiv -\sum_{\{\sigma,z\}} \rho(\{\sigma,z\}) \ln\rho(\{\sigma,z\})$, to a set of clusters with a fixed maximal size. Here we choose this set to be made of all elementary hexagons in the system and all their subclusters, i.e. we take the elementary hexagons, made of six neighbouring triangles, as the largest clusters. We thus use the truncated entropy

$$S_{\mathrm{CVM}} = \sum_{\text{hexagons H}} S_{\mathrm{H}} - \sum_{\text{pairs P}} S_{\mathrm{P}} + \sum_{\text{triangles T}} S_{\mathrm{T}}. \tag{4.6}$$

Here we call $S_{\mathrm{H}} = -\rho_{\mathrm{H}} \ln(\rho_{\mathrm{H}})$ the entropy obtained from the reduced density ρ_{H} for a given hexagon, and similarly for S_{P} and S_{T}. Due to the overlap of neighbouring hexagons, we must subtract the contribution of pairs of neighbouring triangles to avoid overcounting. Similarly, we must add back the contribution of single triangles to account for the overlap of neighbouring pairs. We assume, moreover, that the reduced density ρ_{H} is the same for each hexagon, i.e. that the distribution is translationally invariant. The variational principle will then be applied to this common reduced density matrix associated with the hexagons, which we write as

$$\rho_6(\sigma_1,\sigma_2,\sigma_3,\sigma_4,\sigma_5,\sigma_6,z_1,z_2,z_3,z_4,z_5,z_6), \tag{4.7}$$

with the notation of Fig. 4 for the σ and z variable on a hexagon. In particular, we choose a numbering such that odd indices refer to triangles of subset A and even indices to triangles of subset B. The above reduced density matrix represents the probability for one hexagon to have fixed values of σ and z. It is non-zero only for the allowed sets of σ and z satisfying the two basic folding rules, and it is normalised to one. We also introduce the two-point and one-point functions to account for S_{P} and S_{T} in (4.6):

$$\begin{aligned}\rho_2(\sigma_1,\sigma_2,z_1,z_2) \equiv \tfrac{1}{6} \sum_{\substack{\sigma_3,\sigma_4,\sigma_5,\sigma_6\\ z_3,z_4,z_5,z_6}} \Big[&\rho_6(\sigma_1,\sigma_2,\sigma_3,\sigma_4,\sigma_5,\sigma_6,z_1,z_2,z_3,z_4,z_5,z_6)\\ &+\rho_6(\sigma_3,\sigma_2,\sigma_1,\sigma_4,\sigma_5,\sigma_6,z_3,z_2,z_1,z_4,z_5,z_6)\\ &+\rho_6(\sigma_3,\sigma_4,\sigma_1,\sigma_2,\sigma_5,\sigma_6,z_3,z_4,z_1,z_2,z_5,z_6)\\ &+\rho_6(\sigma_3,\sigma_4,\sigma_5,\sigma_2,\sigma_1,\sigma_6,z_3,z_4,z_5,z_2,z_1,z_6)\\ &+\rho_6(\sigma_3,\sigma_4,\sigma_5,\sigma_6,\sigma_1,\sigma_2,z_3,z_4,z_5,z_6,z_1,z_2)\\ &+\rho_6(\sigma_1,\sigma_6,\sigma_3,\sigma_4,\sigma_5,\sigma_2,z_1,z_6,z_3,z_4,z_5,z_2)\Big]\end{aligned} \tag{4.8}$$

and

$$\rho_{1A}(\sigma_1, z_1) \equiv \sum_{\sigma_2, z_2} \rho_2(\sigma_1, \sigma_2, z_1, z_2),$$
$$\rho_{1B}(\sigma_2, z_2) \equiv \sum_{\sigma_1, z_1} \rho_2(\sigma_1, \sigma_2, z_1, z_2). \tag{4.9}$$

The two-point function ρ_2 is constructed to be invariant under rotations of the hexagon by $\frac{2}{3}\pi$, i.e. by those rotations which leave the two subsets A and B invariant. Using the CVM equation below, this will in turn imply that the six-point function ρ_6 itself has this $\frac{2}{3}\pi$ rotational symmetry. In (4.9) we have introduced two site density matrices, ρ_{1A} and ρ_{1B}, corresponding to the two subsets A and B.

Noting that the numbers N_H, N_P, N_{TA} and N_{TB} of hexagons, pairs and triangles of the subsets A and B, respectively, satisfy $N_P/N_H = 3$, $N_{TA}/N_H = N_{TB}/N_H = 1$, one finds the following approximate CVM free energy *per hexagon*:

$$\begin{aligned} f(\rho_6(\{\sigma_i\}, \{z_i\})) = &-K \sum_{\{\sigma,z\}} \sigma_1\sigma_2(1 + 2z_1z_2)\rho_2(\sigma_1, \sigma_2, z_1, z_2) + \lambda \sum_{\{\sigma,z\}} \rho_6 \\ &+ \sum_{\{\sigma,z\}} (\rho_6 \ln \rho_6) - 3 \sum_{\{\sigma,z\}} (\rho_2 \ln \rho_2) + \sum_{\{\sigma,z\}} (\rho_{1A} \ln \rho_{1A}) \\ &+ \sum_{\{\sigma,z\}} (\rho_{1B} \ln \rho_{1B}), \end{aligned} \tag{4.10}$$

which is a functional of $\rho_6(\{\sigma_i\}, \{z_i\})$ only (by implicit use of Eqs. (4.8) and (4.9)), to be minimised with respect to $\rho_6(\{\sigma_i\}, \{z_i\})$. Here λ is a Lagrange multiplier which ensures the normalisation of $\rho_6(\{\sigma_i\}, \{z_i\})$ to one. The derivative with respect to a generic element of ρ_6 yields the stationarity conditions

$$\begin{aligned} \rho_6(\{\sigma_i\}, \{z_i\}) = &\exp\left[-\lambda + \tfrac{1}{2}K \sum_{i=1,6} (1 + 2z_iz_{i+1})\sigma_i\sigma_{i+1}\right] \\ &\times \Big[\rho_2(\sigma_1, \sigma_6, z_1, z_6)\, \rho_2(\sigma_1, \sigma_2, z_1, z_2)\, \rho_2(\sigma_3, \sigma_2, z_3, z_2) \\ &\times \rho_2(\sigma_3, \sigma_4, z_3, z_4)\, \rho_2(\sigma_5, \sigma_4, z_5, z_4)\, \rho_2(\sigma_5, \sigma_6, z_5, z_6)\Big]^{1/2} \\ &\times \Big[\rho_{1A}(\sigma_1, z_1)\, \rho_{1B}(\sigma_2, z_2)\, \rho_{1A}(\sigma_3, z_3)\, \rho_{1B}(\sigma_4, z_4) \\ &\times \rho_{1A}(\sigma_5, z_5)\, \rho_{1B}(\sigma_6, z_6)\Big]^{-1/3}, \end{aligned} \tag{4.11}$$

with the convention $\sigma_7 = \sigma_1$, $z_7 = z_1$.

One can solve this set of equations, with the definitions of Eqs. (4.8) and (4.9), by iteration. Starting from some assumed form for ρ_2 and iterating the above equation, ρ_6 converges to a solution of (4.11) which is, moreover, a local *minimum* of the approximate free energy (4.10). At each step, the normalisation condition is imposed by adjusting the Lagrange multiplier λ.

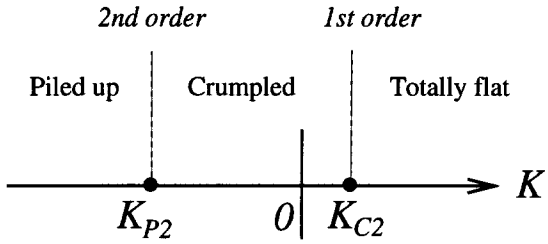

Fig. 8. The phase diagram in the bending rigidity K of the 2D folding problem.

In practice, we expect that the expectation values P, O and T of Eqs. (4.1) are the same for negative K when calculated on the subset A only or the subset B only. This implies $\rho_{1A}(\sigma, z) = \rho_{1B}(-\sigma, z)$. It is thus more convenient to use the variable σ_{st}, instead of σ, and to introduce a single one-point function $\rho_1^{st}(\sigma_{st}, z) \equiv \rho_{1A}(\sigma_{st}, z) = \rho_{1B}(-\sigma_{st}, z)$ which is independent of the subset A or B. Eq. (4.11), which is a set of 96×4 coupled equations, can be reduced to a much smaller set of equations by introducing appropriate ratios of six-point functions and noting that some of these ratios are identical. For instance:

$$\frac{\rho_6(++-+--,+++++)}{\rho_6(--+-++,+++++)} = \frac{\rho_6(---+++,+++++)}{\rho_6(+++---,+++++)} = \frac{\rho_2(-+,++)}{\rho_2(+-,++)} \left(\frac{\rho_{1A}(+,+)\,\rho_{1B}(-,+)}{\rho_{1A}(-,+)\,\rho_{1B}(+,+)} \right)^{1/3}. \tag{4.12}$$

We can then use an appropriate parametrisation of the six-point function in terms of a small number of independent ratios. For these we get a much smaller closed set of coupled equations which can be solved numerically by recursion. In practice, we used a set of 9 independent ratios.

4.2. *Results of the CVM for the 2D (arbitrary K) and 3D (positive K) folding problems*

Before we present our results for the 3D folding problem at negative K, let us briefly recall the results which have been obtained in Ref. [11], where the CVM was applied to the 2D folding problem (i.e. to the planar 11-vertex submodel) with arbitrary K, and those of Ref. [13] for the full 3D folding problem in the FCC lattice with positive K.

For the 2D folding problem, characterised in our notation by $z = +1$ everywhere, the CVM predicts two transitions, as depicted in Fig. 8. A first-order crumpling transition at $K_{C2} \sim 0.1013$ separates a large positive K *totally flat* phase with $\sigma = +1$ everywhere from a low-$|K|$ crumpled phase with $\langle\sigma\rangle = 0$. This latter phase also has $\langle\sigma_{st}\rangle = 0$ and persists with decreasing K to negative values until $K_{P2} \sim -0.284$, where a second-order piling transition takes place[6]. For $K < K_{P2}$, the system develops a non-zero value of $\langle\sigma_{st}\rangle$, indicating a tendency for triangles to pile on top of each other. At $K = 0$, the

[6] An exact formula for K_{P2} can be found in Ref. [19].

number of folded states for N triangles is found to grow like q^N with $q = \frac{1}{3}\sqrt{13} \sim 1.202$, to be compared with the exact value $q = \sqrt{3}\,\Gamma(\frac{1}{3})^{3/2}/2\pi \sim 1.208$. Note that this phase diagram is also found by another approach to the problem using a transfer matrix formalism [6].

We stress here that, thanks to the duality transformation, this phase diagram applies to the 11-vertex model describing folding on a single tetrahedron. The only modification is that the energy difference between the two types of allowed folds, which is $K - (-K) = 2K$ in the planar problem, is now $-\frac{1}{3}K - (-K) = \frac{2}{3}K$. The phase diagram of the tetrahedral folding problem is thus exactly the same as that of the planar folding problem with $K \to 3K$. For instance the piling transition now occurs at $K \sim -3\times 0.284 = -0.852$.

For the 3D folding problem in the FCC lattice, the CVM method has been used in Ref. [13] for positive K only. There it was found that, as in the 2D case, a first-order crumpling transition takes place, now at a larger value $K_{C3} \sim 0.1855$ between a large K totally flat phase with $z = \sigma = +1$ everywhere, and a crumpled state with $\langle z \rangle = \langle \sigma \rangle = 0$. A remarkable difference is that the low-K crumpled state now has $\langle \sigma_{\rm st} \rangle$ non-zero. For instance, at $K = 0$, one gets $\langle \sigma_{\rm st} \rangle \simeq 0.87456$. As mentioned at the beginning of this section, this indicates a strong preference for the lattice to wrap on octahedra. This non-zero value of the staggered σ variable is not surprising in the sense that the 3D folding problem in the FCC lattice may be formulated approximately as a 2D folding problem with a staggered magnetic field (see Ref. [12]). Furthermore, a comparison, at $K = 0$, of the entropy factor q for the full 3D folding problem (estimated to be 1.428 by the CVM and 1.43 by a transfer matrix approach [12]) with that of the single octahedron folding problem ($q = \sqrt{2} \sim 1.414$) shows that the wrapping of octahedra is the entropically dominant folding process at zero bending rigidity.

4.3. 3D folding at negative K

We now present our results for the CVM applied to the full 3D folding problem in the FCC lattice, with *negative* K. Our main result is the existence of two separate geometrical transitions with increasing $|K|$: a first discontinuous transition at $K = K_{G3} \sim -0.294$ separates a phase where the triangular lattice is preferentially wrapped around octahedra from a phase where it is preferentially wrapped around tetrahedra. A second continuous transition at $K = K_{P3} \sim -0.852$ separates this latter phase from a phase of complete folding of the lattice on top of a single triangle.

The first sign of these transitions can be seen directly by looking at the evolution with K of the relative proportions of the four types of folds averaged over the folded states of the lattice. These proportions are displayed in Fig. 9. At $K = 0$, the fraction of acute folds and no-folds is identical, as a consequence of duality. Together they represent, however, only 5% of all folds and the statistics is dominated by complete and obtuse folds, indicating a phase of wrapping of octahedra. This domination of complete and obtuse folds persists in the range $K_{G3} < K \leqslant 0$. At $K = K_{G3}$, all proportions show a discontinuity. For $K < K_{G3}$, the statistics is now dominated by complete and acute folds, indicating a phase of wrapping of tetrahedra. The proportion of the other types of

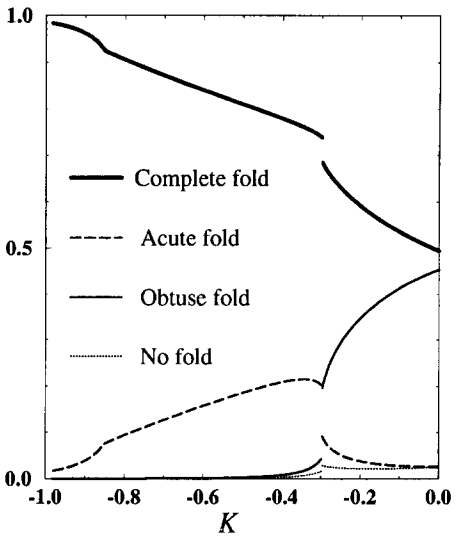

Fig. 9. The average proportions of the four types of folds, as a function of K.

folds becomes essentially zero for $K \sim -0.6$. The proportion $p(K)$ of complete folds (respectively $1-p(K)$ of acute folds) then increases (respectively decreases) smoothly with increasing $|K|$. This domination of complete folds is enhanced at $K = K_{P3}$, where a discontinuity in the slope of $p(K)$ signals a continuous transition.

A more detailed description is provided by examining the three order parameters O, T, and P defined in (4.1), whose values, displayed in Fig. 10, clearly indicate three separate phases. At low $|K|$ the system is preferentially wrapped around octahedra, i.e. is in a phase with a non-zero value of the octahedral order parameter O, while the other two order parameters T and P remain zero. For intermediate $|K|$, the system is preferentially wrapped around tetrahedra, i.e. is in a phase with a non-zero value of the tetrahedral parameter T, while the two other order parameters vanish. The geometrical transition at $K = K_{G3} \sim -0.294$ between these two phases is first order. At large values of $|K|$, the three order parameters are non-zero with $T \simeq +1$ and $O \simeq P$. This clearly indicates a phase where the triangles are preferentially piled up on top of each other. In practice, the tetrahedral order parameter becomes indistinguishable from its saturated value $T = +1$ for $|K| > 0.6$, so that at large $|K|$, the 96-vertex model becomes indistinguishable from the pure tetrahedral 11-vertex model (defined by $\sigma_{\rm st} = z$), which satisfies $O = P$. It is therefore not surprising to recover the second-order piling transition of the 11-vertex model, which, as explained above, occurs at $K_{P3} \sim -3 \times 0.284 = -0.852$.

The final phase diagram of the 3D folding problem of the triangular lattice in the FCC lattice is shown in Fig. 11. When compared with that of the 2D planar folding problem, displayed in Fig. 8, we see that the crumpled phase has been replaced by two geometrical octahedral and tetrahedral phases, separated by a first-order transition. Note that the octahedral phase persists at positive K until the transition point K_{C3} where the totally flat phase is recovered. The passage from the totally flat phase to the piled-up

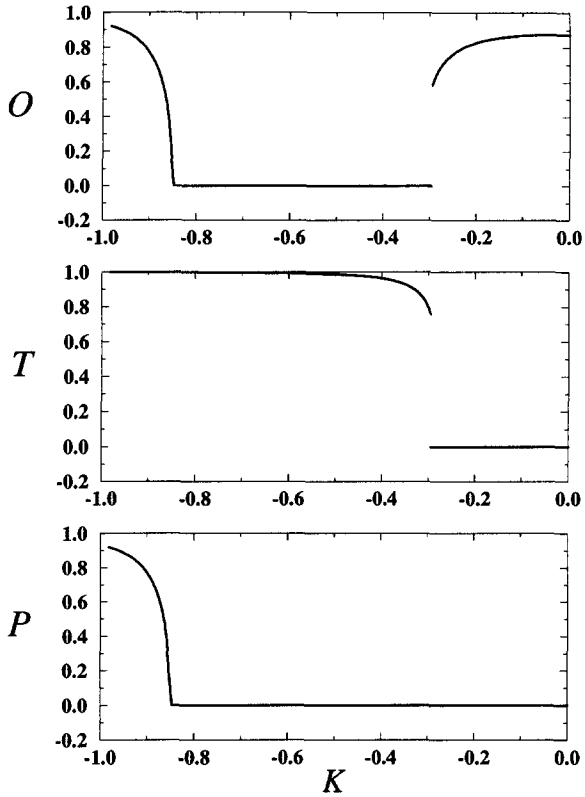

Fig. 10. The octahedral order parameter O, tetrahedral order parameter T and planar order parameter P as a function of the bending rigidity K.

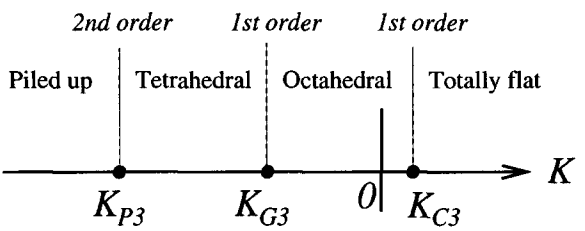

Fig. 11. The phase diagram in the bending rigidity K of the 3D folding problem in the FCC lattice.

phase, which involved two transitions in the 2D case, now requires three transitions.

It is interesting to compare our model with the Ashkin–Teller model [20] defined in terms of two *unconstrained* Z_2 variables σ_{st} and z with pair energy:

$$E = -K_O(\sigma_{st})_1(\sigma_{st})_2 - K_P z_1 z_2 - K_T(z\sigma_{st})_1(z\sigma_{st})_2, \tag{4.13}$$

involving three energy parameters $K_{O,P,T}$. Note that, despite the apparent asymmetry, the three Z_2 variables σ_{st}, z and $z\sigma_{st}$ are actually exactly on the same footing: for any two of them, the third one is simply the product of these two. Our energy (2.5) corresponds to a trivial case $(K_O, K_P, K_T) = (-\frac{1}{3}K, 0, -\frac{2}{3}K)$ where one of the coupling

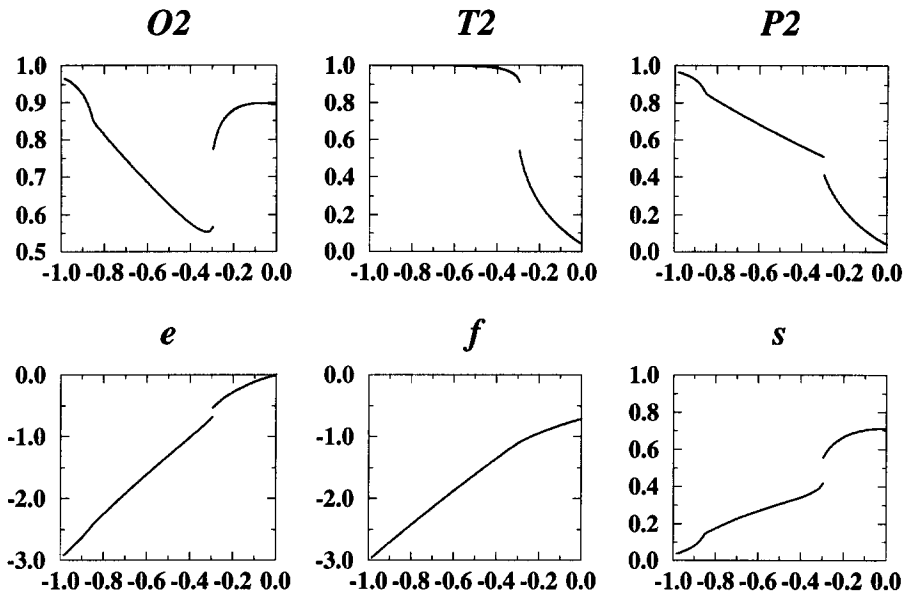

Fig. 12. The two-point functions $O2$, $T2$ and $P2$ and the energy e, free energy f and entropy $s = e - f$ per hexagon, as a function of the negative bending rigidity K.

constants vanishes. The *unconstrained* system then translates into two independent Ising models with two continuous transitions with increasing $|K|$ describing the successive symmetry breakings of first $\langle \sigma_{\rm st} z \rangle$ at $K = -\frac{3}{2}K_c$ and then of $\langle \sigma_{\rm st} \rangle$ at $K = -3K_c$, while $\langle z \rangle = \langle \sigma_{\rm st} \rangle \langle z\sigma_{\rm st} \rangle$ for all K. Here $K_c = -(\frac{1}{2}) \ln(2 - \sqrt{3}) \simeq 0.658$ is the critical Ising coupling on the honeycomb lattice. In particular, at low $|K|$, all order parameters vanish. We see that the constraints (2.1) and (2.3) on the $\sigma_{\rm st}$ and z variables modify this picture by replacing the first continuous transition by a discontinuous one and by giving rise to a low-$|K|$ phase where $\langle \sigma_{\rm st} \rangle$ is non-zero. In this phase, the origin of the symmetry breaking in the variable $\sigma_{\rm st}$ is clearly entropic. Indeed it allows for a gain in entropy from the z variable as the second basic folding rule is less constraining when the σ variables alternate on the lattice.

Since we can extract the two-point function from the CVM, we have access to the nearest-neighbours correlations $O2$, $T2$ and $P2$ defined in (4.2), as well as to the average energy *per hexagon*:

$$e = K(O2 + 2T2). \tag{4.14}$$

We also have access to the free energy f per hexagon and to the entropy part $s = e - f$. These quantities are displayed in Fig. 12 as a function of K.

4.4. *The transfer matrix approach*

The CVM gives only an approximation to the exact statistics of the problem and it is difficult to estimate quantitatively possible systematic errors of the method. In

particular, due to the truncation of the free energy functional to finite clusters, we cannot even ensure that the CVM free energy is bounded from below by the true free energy. It is thus important to compare the CVM results with those of other methods. In the case of 2D folding, a formulation of the problem was given in terms which allows for the use of a transfer matrix method [6], leading to a very satisfactory comparison with the CVM approach. The same method was generalised for the 3D folding problem at $K = 0$ in Ref. [12]. In this section, we present the results of a transfer matrix study of the 3D folding problem at negative bending rigidity K.

In the transfer matrix formalism, the folding partition function $Z_L(K)$ of an infinite strip with a finite width L and with rigidity K is given by

$$Z_L(K) = \lim_{n\to\infty} [\mathrm{Tr}(T_L(K)^n)]^{1/n}, \tag{4.15}$$

where $T_L(K)$ is the row to row transfer matrix of the system. The state of a row is specified by the $2 \times 2L$ triangle variables σ_i and z_i in the row. We use free boundary conditions which allow folds to escape from the strip at its boundary. In the folding problem, a transfer matrix element from the lower row $\{\sigma, z\}$ to the upper row $\{\sigma', z'\}$

$T_{L\{\sigma,z\},\{\sigma',z'\}} =$ 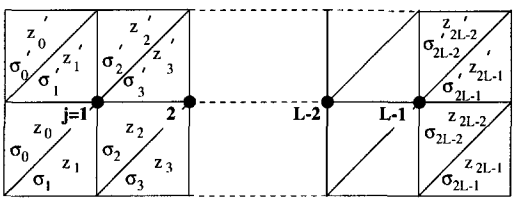

(4.16)

is non-zero *iff* the two basic folding rules (2.1) and (2.3) are satisfied around each of the vertices $j = 1, \ldots, L-1$; if so, it is equal to $\exp(-E)$, where E is the folding energy (2.5), proportional to K, for all pairs of neighbouring triangles in the two rows. This method has been extensively described in Ref. [12] for the 3D folding *without* rigidity ($K = 0$). The question of the rigidity has been addressed in Ref. [6] for the 2D folding problem. The reader is referred to these articles for further details on the method.

As usual, we must extract the largest eigenvalue (and its eigenvector) of the matrix $T_L(K)$. The main difficulty is that the size of this matrix increases exponentially with L like $4^{2L} \times 4^{2L}$. Also, due to the chirality in the representation of the triangular lattice as a square lattice in (4.16), the transfer matrix is not directly symmetric, which requires the use of both left and right eigenvectors. Fortunately, the vanishing of all elements which do not satisfy the basic folding rules makes the matrix very sparse. With the Cray C94 of CEA-Grenoble, we have been able to reach $L = 6$ with one gigabyte of memory. By comparison, in 2D folding, the size of the matrix was $2^{2L} \times 2^{2L}$ and the width L could be doubled. These computations are exact, in the sense that the precision is limited by the numerical precision of the computer; no approximations are made with this method. Of course, the infinite lattice folding is recovered only in the limit where $L \to \infty$.

Strictly speaking, an infinite strip with finite width is a one-dimensional system which has no phase transition and all order parameters vanish due to the global symmetry under

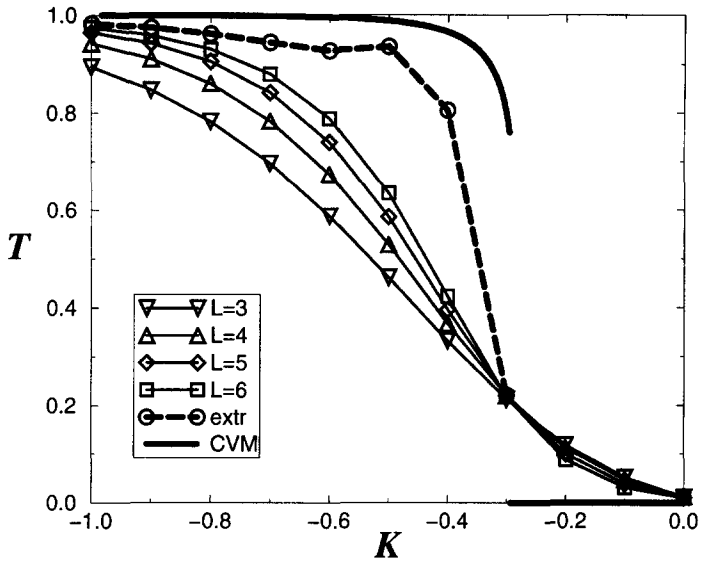

Fig. 13. The results of the transfer matrix method for the tetrahedral order parameter T as a function of (negative) K. The figure displays the results for strips of size $L = 3,4,5,6$ as well as the extrapolation to infinite L (see text). By comparison, the corresponding result of the CVM is also indicated.

reversal of all spins. The order parameters, however, can be estimated by weakly breaking the symmetry by first fixing the (σ, z) variables of, say, the most central triangle of a row $i = L$ and by averaging each order parameter on the other triangles. In practice, it is useful to restrict oneself to triangles j with $|j - i| > 1$, i.e. to triangles which are not nearest neighbours of i. In fact, the contribution of neighbouring triangles is less significant because the short-range correlations are always large even in a disordered phase. To summarise, we measure $X_L = 1/(2L-3) \sum_{j:|j-L|>1} \langle x_L x_j \rangle$ as an estimate for the order parameter $X = \langle x \rangle$ to be considered ($x = \sigma_{\rm st}, z\sigma_{\rm st}$ or z, i.e. $X = O, T$ or P).

Using the Padé–Shanks transformation (see Ref. [21]), the finite size effects can be reduced. Given three values X_4, X_5, X_6 obtained for sizes $L = 4,5,6$, and supposing the convergence is exactly exponential, the extrapolated value is $X_\infty = (X_4 X_6 - X_5^2)/(X_4 + X_6 - 2X_5)$.

In Fig. 13, the tetrahedral order parameter T, estimated as described above, is plotted as a function of the negative rigidity K. For finite width $L = 6$, the first-order transition predicted by the CVM is smoothed by finite size effects. The extrapolation $L \to \infty$, however, clearly shows a rapid change around $K = -0.3$. Unfortunately, the maximum size $L = 6$ is too small to allow a precise determination of K_{G3} or even the order of the transition. We can still estimate K_{G3} roughly by considering the point where all curves at finite L seem to intersect. This leads to $K_{G3} \sim -0.3$, in good agreement with the CVM estimate $K_{G3} \sim -0.294$.

For the other order parameters (P and O), the curves are smoother and the predicted transitions less visible. Still, the variations of these order parameters with K are in agreement with the infinite system limit expected from the CVM results. For instance,

we see an intermediate-$|K|$ regime with a low value of O surrounded by a small- and large-$|K|$ regime with a significantly larger value of O, as expected in the presence of an intermediate tetrahedral phase.

Clearly, the exact transfer matrix method is more difficult in the 3D folding case than in the 2D folding case, due to the higher number of states. In the 2D case, the first signal of the continuous piling transition at K_{P2} did not occur until system width $L = 8$. Such a large system size is impractical in the 3D problem. In this context we can conclude that the transfer matrix results do not contradict in any way those of the CVM, which in turn appears to be a much more powerful approach.

5. External fields

In this section, we briefly discuss the consequence of adding external fields coupled to our Z_2 spin variables. The results of this section are again obtained in the framework of the CVM. We add to the pair energy (2.5) the following external field contribution:

$$E_H = -H_O\sigma_{\rm st} - H_T z\sigma_{\rm st} - H_P z, \tag{5.1}$$

with three external fields H_O, H_T and H_P coupled to the order parameters $O = \langle\sigma_{\rm st}\rangle$, $T = \langle z\sigma_{\rm st}\rangle$ and $P = \langle z\rangle$, respectively.

For simplicity, we will discuss in the following the consequence on the negative K phase diagram of having one of these fields non-zero, while the two others are kept equal to zero.

As explained in Section 4.3, in the absence of external field, the system was found to have three phases for negative K. The nature of each phase can be characterised by specifying which of the three order parameters O, T and P are zero or not.

(i) The low-$|K|$ octahedral phase has $O \neq 0$, $P = T = 0$.

(ii) The intermediate-$|K|$ tetrahedral phase has $O = 0$, $P = 0$ and $T \neq 0$.

(iii) The large-$|K|$ piled-up phase has $O \neq 0$, $P \neq 0$ and $T \neq 0$.

We find that the nature of a phase is *unchanged* by the addition of a (small enough) external field H_X if the order parameter X was non-zero in this phase. Here X stands for O, T or P. On the other hand, if X happened to be zero in a phase, then the action of H_X is to make all order parameters non-zero.

For instance, the piled-up phase, which has its three order parameters non-zero, persists in the presence of external fields. In the presence of a non-zero value of H_O, the octahedral phase is preserved but the continuous piling transition is *suppressed.* The original tetrahedral and piled-up phase merge into a single phase with non-zero order parameters O, T and P. This phase can be viewed as a tetrahedral phase with a smoothly increasing piled-up order with increasing $|K|$. The first-order transition, now directly from the octahedral phase to this phase, is slightly shifted to larger values of $|K|$. In the presence of a non-zero value of H_T, the tetrahedral and piled-up phases are not modified and the second-order transition is preserved at its original value of K. This is not surprising since T was already saturated to $T \simeq 1$ in this regime. On

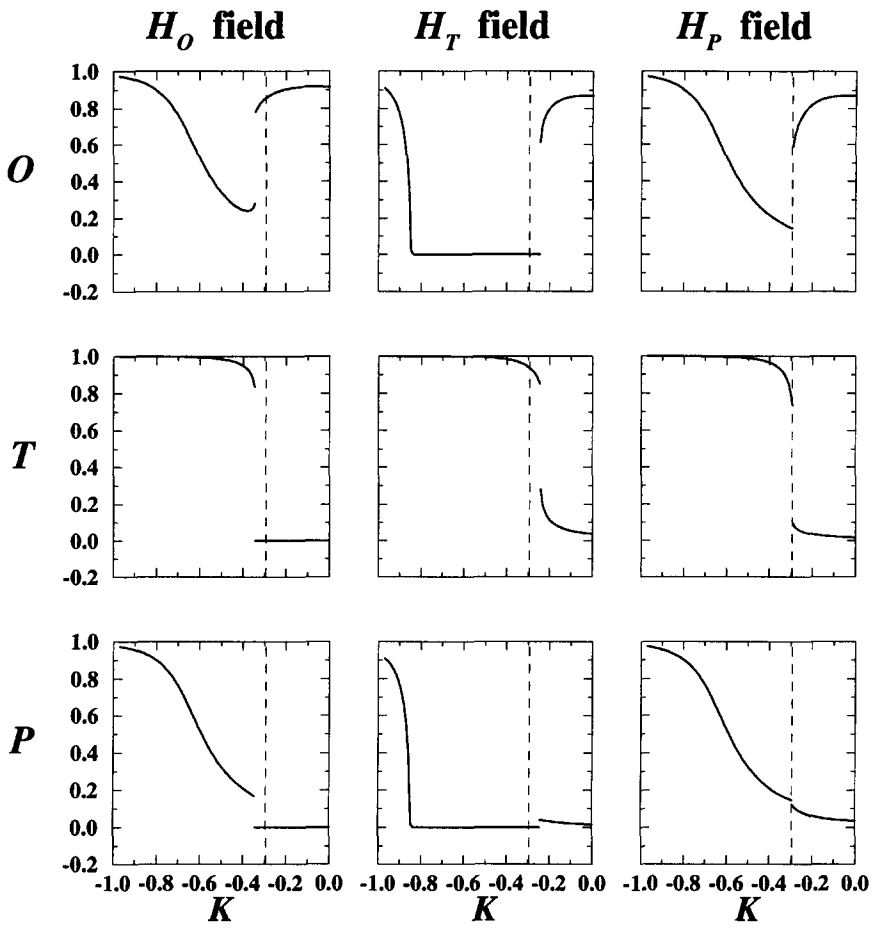

Fig. 14. The variation with the negative bending rigidity K of the three order parameters O, T and P in the presence of a small applied external field. The first (respectively second and third) column corresponds to the application of a positive external field H_O (respectively H_T and H_P). The dashed vertical line indicates the location of the first-order geometrical transition in the absence of external fields.

the other hand, the system develops non-zero order parameters T and P in the low-$|K|$ region, indicating the appearance of a piled-up order in the original octahedral phase. The first-order transition from this phase to the tetrahedral phase is *preserved* (for small enough H_T at least), although slightly shifted to smaller values of $|K|$. Finally, in the presence of a non-zero value of H_P, the three order parameters become non-zero over the whole negative K range. The second-order transition is *suppressed* while the first-order transition now takes place between two phases of the same nature, discriminated only by which fraction of acute or obtuse folds is larger.

The above discussion is illustrated in Fig. 14 where the three order parameters O, P and T and represented as a function of K in the presence of an applied external field H_O, H_T or H_P.

6. Discussion

In this paper, we have studied the folding of the 2-dimensional regular triangular lattice in the 3-dimensional regular Face-Centred Cubic lattice, a problem which can be expressed as a 96-vertex model on the triangular lattice. We considered the case of negative bending rigidity K, where folds are favoured. A special role is played by three classes of elementary objects in the FCC, namely elementary octahedra, tetrahedra and triangles. Indeed, instead of randomly wandering over all sites of the FCC lattice, the system prefers to stay trapped on one class of these objects:

- At low $|K|$, the system is preferentially wrapped on octahedra, characterised by obtuse 109° degree folds.
- At intermediate $|K|$, the system is preferentially wrapped on tetrahedra, with acute 71° folds.
- At large $|K|$, the system is preferentially piled onto single triangles, making complete 0° folds.

This leads to three distinct phases, characterised by the symmetry breakings of appropriate order parameters. These phases are separated by two transitions, a discontinuous one between the octahedral and the tetrahedral phase and a continuous one between the tetrahedral and the piled-up phase. This study completes the previous one at positive K which found a first-order crumpling transition with a large positive K completely flat phase.

Our results were obtained in the framework of the CVM approximation and further corroborated by a transfer matrix approach. At this stage, one may wonder whether the particular form (2.4) of the bending energy is crucial for our results. We expect that, as long as the energy is a monotonic function of the angle of the fold which, moreover, favours folding, the above scenario will continue to hold. One may also question the validity of the CVM approximation in a very constrained problem where folds are, moreover, expected to propagate throughout the entire lattice, far beyond the size of the basic cluster of the CVM. Actually, as explained in Ref. [5] for the 2D folding problem, the necessity for folds to propagate through the lattice is entirely encoded in the particular form of the 96 local hexagonal configurations *and* the matching condition for the folds on links which are common to two overlapping hexagons. These two ingredients are properly taken into account by the CVM. We thus believe that this method does indeed account for the propagation of folds and therefore gives reliable results concerning the phase diagram and the transitions separating distinct phases. Nevertheless, as for any mean field approach, the method gives only trivial critical exponents for the continuous piling transition, whose true universality class is therefore still to be determined. A CVM approach with larger clusters would not help to resolve this issue and we believe that the restriction to hexagonal clusters is probably the most efficient choice in terms of simplicity. On the other hand, a transfer matrix method, which is exact for strips of finite size L does not allow us to reach large enough system sizes to allow a reliable continuum ($L \to \infty$) extrapolation. It is thus a challenge to find alternative methods for a more refined study of this problem.

Finally, the particular sequence of folding involving octahedra and tetrahedra is clearly intimately linked to the structure of the FCC target space where the 3D rotational symmetry has been explicitly broken to a smaller (cubic) symmetry. On the other hand, the piled-up phase with alternating normal vectors on neighbouring triangles is likely to exist even if the target space is continuous. One may wonder whether the folding of the triangular lattice in a continuous 3D space also gives rise to intermediate phases with particular broken symmetries, not necessarily related of course to the FCC cubic symmetry.

Acknowledgements

The research of M.B. was supported by the Department of Energy, USA, under contract No. DE-FG02-85ER40237. This work is partially supported by the JSPS fellowship for Junior Scientists. We thank J.-M. Normand for a critical reading of the manuscript.

References

[1] D.R. Nelson, T. Piran and S. Weinberg, eds., Statistical Mechanics of Membranes and Surfaces, Proceedings of the fifth Jerusalem Winter School for Theoretical Physics (World Scientific, Singapore, 1989).
[2] F. David, P. Ginsparg and J. Zinn-Justin, eds., Fluctuating Geometries in Statistical Mechanics and Field Theory, Les Houches Session LXII (Elsevier Science, Amsterdam, 1996) (http://xxx.lanl.gov/lh94).
[3] F. David and E. Guitter, Europhys. Lett. 5 (1988) 709.
[4] Y. Kantor and M.V. Jarić, Europhys. Lett. 11 (1990) 157.
[5] P. Di Francesco and E. Guitter, Europhys. Lett. 26 (1994) 455 (cond-mat/9402058).
[6] P. Di Francesco and E. Guitter, Phys. Rev. E 50 (1994) 4418 (cond-mat/9406041).
[7] R.J. Baxter, J. Math. Phys. 11 (1970) 784; J. Phys. A: Math. Gen. 19 (1986) 2821.
[8] N.Yu. Reshetikhin, J. Phys. A 24 (1991) 2387.
[9] H.W.J. Blöte and B. Nienhuis, Phys. Rev. Lett. 72 (1994) 1372.
[10] D.A. Huse and A.D. Rutenberg, Phys. Rev. B 45 (1992) 7536.
[11] E. Cirillo, G. Gonnella and A. Pelizzola, Phys. Rev. E 53 (1996) 1479 (hep-th/9507161).
[12] M. Bowick, P. Di Francesco, O. Golinelli and E. Guitter, Nucl. Phys. B 450 [FS] (1995) 463 (cond-mat/9502063).
[13] E. Cirillo, G. Gonnella and A. Pelizzola, Phys. Rev. E 53 (1996) 3253 (hep-th/9512069).
[14] M. Bowick, P. Di Francesco, O. Golinelli and E. Guitter, Discrete folding, to appear in the Proceedings of the 4th Chia Meeting on Condensed Matter and High-Energy Physics, September 4–8, 1995 (World Scientific, Singapore) (cond-mat/9610215).
[15] F.F. Abraham and D.R. Nelson, J. Phys. (Paris) 51 (1990) 2653.
[16] R. Kikuchi, J. Chem. Phys. 60 (1974) 1071.
[17] T. Morita, Prog. Theor. Phys. 103 (1984) 103.
[18] G. An, J. Stat. Phys. 52 (1988) 727.
[19] P. Di Francesco, E. Guitter and S. Mori, Phys. Rev. E 55 (1997) 237 (cond-mat/9607077).
[20] R.J. Baxter, Exactly Solved Models in Statistical Mechanics (Academic Press, New York, 1982).
[21] C. Brezinski and M. Redivo Zaglia, Extrapolation Methods (North-Holland, Amsterdam, 1991).